IEEE Access
Multidisciplinary | Rapid Review | Open Access Journal

Received July 29, 2019, accepted August 2, 2019, date of publication August 6, 2019, date of current version August 21, 2019.

Digital Object Identifier 10.1109/ACCESS.2019.2933584

Optimal Sensor Deployment and Velocity Configuration With Hybrid TDOA and FDOA Measurements

WEIJIA WANG, PENG BAI, YUBING WANG, XIAOLONG LIANG, AND JIAQIANG ZHANG
Air Traffic Control and Navigation College, Air Force Engineering University, Xi'an 710051, China

Corresponding author: Xiaolong Liang (afeu_lxl@sina.com)

This work was supported in part by the National Natural Science Foundation of China (NSFC) under Grant 61703427 and Grant 61502522.

ABSTRACT Source localization based on the hybrid time-difference-of-arrival (TDOA) and frequency-difference-of-arrival (FDOA) measurements from distributed sensors is an essential problem in wireless sensor networks (WSNs). In this paper, we mainly study the optimal sensor deployment and velocity configuration of UAV swarms mounted with TDOA and FDOA based sensors. Explicit solutions of optimal sensor deployment and velocity configuration are acquired in both static and movable source scenarios based on the Fisher information matrix (FIM). Both centralized and decentralized localization are explored to meet different types of localization methods. Path planning problem of UAV swarms in TDOA/FDOA localization is also studied with constraints. Simulations verify its efficiency with path planning in TDOA and FDOA localization.

INDEX TERMS Time-difference-of-arrival (TDOA), frequency-difference-of-arrival (FDOA), sensor deployment, fisher information matrix, path planning.

I. INTRODUCTION

Localization of a radio frequency (RF) with static and movable sensors has received significant interest in both civil and defense applications, such as search, rescue, and surveillance. The measurements from spatially distributed sensors are the efficient way to estimate the location of a non-cooperative source. Several types of measurements can be used such as time-difference-of-arrival (TDOA) [1], angle-of-arrival (AOA) [2], received signal strength (RSS) [3], or a combination of them. Frequency differences of arrival (FDOA) can also be applied to improve localization accuracy, when the source and the sensors are relatively moving. Here, in this paper, we consider the source localization with hybrid TDOA and FDOA measurements.

Many TDOA/FDOA localization algorithms have been studied in the literatures, e.g., two-step weighted least square (WLS) method, constrained quadratic programming [4], pseudolinear estimation [5] and the constrained weighted least squares (CWLS) method [6]. Kalman filters based on TDOA and FDOA measurements are also applied in [7], [8].

The associate editor coordinating the review of this manuscript and approving it for publication was Qingchun Chen.

It is well known that the geometric placement of sensors in the localization can significantly influence the localization accuracy. Bishop and Jensfelt [9]–[12] firstly studied the optimal deployment of homogeneous sensors, i.e., AOA, RSS and TOA (time-of-arrival), respectively. The determinant of FIM was applied as the optimal criterion to analysis the different geometries in different types of localization. Yang [13] and Rui and Ho [14] studied the optimal deployment of TDOA localization by minimizing the trace of Cramer-Rao low bound (CRLB). Zhao *et al.* [15] cast the optimal homogeneous sensor deployment problem into parameter optimization problem and frame theory was applied to solve it.

Recently, placement of the heterogeneous sensors has drawn a considerable amount of attention. Yang *et al.* [16] preliminarily considered the two-group and paired strategies in heterogeneous sensor localization, which was also based on the FIM in hybrid TOA and AOA localization. Lee *et al.* [17] studied the hybrid AOA and TOA localization on unmanned aerial vehicle (UAV) platforms. Meng *et al.* [18] studied explicit characterizations of the optimal geometries in hybrid TOA, AOA and TDOA localization. Liang and Jia [19] proposed the optimal placements of TOA/AOA/RSS sensors with distance-dependent noise and

constrained regions were studied based on the Cramer-Rao low bound (CRLB). Moreover, other types of hybrid localization i.e., hybrid AOA/RSS [20], AOA/FDOA [21] are also discussed.

Unlike other types of localization methods, FDOA allows for estimating the velocity of a moving source. Geometric dilution of precision (GDOP) is another criterion considered in a number of papers. In hybrid TDOA/FDOA localization, Guo *et al.* [22] studied the optimal deployment of a dual satellite system through geometric dilution of precision (GDOP). The performances of satellite altitude, satellite distance as well as velocities are considered. Kim *et. al.* [23], [24] studied the relationship between the linear velocity and localization accuracy. Some fixed sensor geometries and manoeuvre strategies are chosen for localization. Hmam [25] mainly studied the velocity configurations for sensor pairs to achieve optimal localization of a stationary source.

In this paper, we extend the two sensors to sensor networks. The optimal deployments and velocity configuration of both centralized and decentralized localization are considered based on FIM in the static source scenario. Different with the other types of localization methods, source localization that based on the FDOA measurements needs more control on the sensor velocities. We find that the optimal deployment and velocity configuration is related to both the angular separation and angular velocities with respect to the source. We also propose preliminary analysis on the optimal deployment and velocity configuration in movable source scenario. For a better visibility of sources, we extend our work on path planning of UAV swarms, which are mounted with TDOA/FDOA sensors. FIM and posterior error covariance is adopted as the objective function for sensor-source geometry and velocity optimization. And the constrained nonlinear optimization problem is studied to obtain a sequence of optimized waypoints for UAV swarms.

The rest of this paper is organized as follows. Section 2 presents the problem statement in TDOA/FDOA localization. Section 3 and 4 provide the theoretical analysis on sensor pair geometries, for both centralized and decentralized localization in static and movable source scenarios, respectively. In section 5, path planning problem is considered. Section 6 provides some examples to verify the findings in Section 3 and 4. Section 7 concludes the paper.

II. PROBLEM STATEMENT

We consider a two-dimensional (2-D) scenario where M moving sensors are applied to estimate the position $\mathbf{x}_p = \left[x_p, y_p\right]^T$ and velocity $\mathbf{v}_p = \left[v_{px}, v_{py}\right]^T$ of a source using TDOA and FDOA measurements. The moving sensor positions $\mathbf{x}_i = [x_i, y_i]^T$ and velocities $\mathbf{v}_i = \left[v_{ix}, v_{iy}\right]^T$ are assumed known. Our aim is to obtain a higher localization and tracking accuracy from TDOA and FDOA measurements through pursuing optimal sensor deployment and velocity configuration.

For sensor i and j, the TDOA measurement in the range domain is obtained by:

$$r_{ij} = r_{ti} - r_{tj}, \quad i, j \in \{1, \ldots, M\} \wedge j \neq i, \tag{1}$$

where $r_{ti} = \left\|\mathbf{x}_p - \mathbf{x}_i\right\|$ is the distance between the source and TDOA sensor. Let v_i be the TOA estimation error, which is assumed to be Gaussian. Let σ_{ri}^2 denote the measurement variance of the i-th receiver of the UAV platform, then the measurement noise $v_{ij} = v_i + v_j$ is composed of the noises at the two associated receivers and has the covariance $\sigma_{ri}^2 + \sigma_{rj}^2$.

Therefore, the TDOA measurement vector at the time k is given by:

$$\widehat{\mathbf{r}} = \left[\hat{r}_{21}, \hat{r}_{31}, \ldots, \hat{r}_{M1}\right]^T = \mathbf{r}(\mathbf{x}_p) + \mathbf{w}_r, \tag{2}$$

where $\mathbf{w}_r = [v_{12}, v_{13}, \ldots, v_{1M}]^T$ with covariance matrix $\mathbf{\Sigma}_r$.

By taking the time derivative, the range rate of the i-th sensor and the source can be written as

$$\dot{r}_i = \frac{\left(\mathbf{v}_p - \mathbf{v}_i\right)^T \left(\mathbf{x}_p - \mathbf{x}_i\right)}{r_i} = \left(\mathbf{v}_p - \mathbf{v}_i\right)^T \mathbf{u}_i, \tag{3}$$

where $\mathbf{u}_i$ is a unit vector of the radius vector. Thus the Doppler-shift measurement is

$$f_i = \frac{f_0}{c} \left(\mathbf{v}_p - \mathbf{v}_i\right)^T \mathbf{u}_i. \tag{4}$$

Therefore, the FDOA measurement between the i-th and the j-th sensor is

$$f_{ij} = f_i - f_j = \frac{f_0}{c} \left(\left(\mathbf{v}_p - \mathbf{v}_i\right)^T \mathbf{u}_i - \left(\mathbf{v}_p - \mathbf{v}_j\right)^T \mathbf{u}_j\right), \tag{5}$$

where f_0 is the carrier frequency of the signal, c is the speed of the signal propagation.

Similarly, we assume that the FDOA measurements follow a Gaussian distribution. Then the FDOA measurement vector is given by

$$\widehat{\mathbf{f}} = \left[\hat{f}_{21}, \hat{f}_{31}, \ldots, \hat{f}_{M1}\right]^T = \mathbf{f}(\mathbf{x}_p) + \mathbf{w}_f, \tag{6}$$

where, $\mathbf{w}_f$ is the measurement error with covariance matrix $\mathbf{\Sigma}_f$.

Combining the observed TDOA and FDOA measurements, the total measurements vector is given by

$$\widehat{\mathbf{z}} = \mathbf{z} + \mathbf{w} = \begin{bmatrix} \mathbf{r} \\ \mathbf{f} \end{bmatrix} + \begin{bmatrix} \mathbf{w}_r \\ \mathbf{w}_f \end{bmatrix}. \tag{7}$$

The corresponding measurement noise vector is

$$\mathbf{\Sigma} = E\left[\mathbf{w}\mathbf{w}^T\right] = E\left[\begin{bmatrix} \mathbf{w}_r^T & \mathbf{w}_f^T \end{bmatrix}^T \begin{bmatrix} \mathbf{w}_r^T & \mathbf{w}_f^T \end{bmatrix}\right] = \begin{bmatrix} \mathbf{\Sigma}_r & 0 \\ 0 & \mathbf{\Sigma}_f \end{bmatrix}. \tag{8}$$

III. OPTIMAL DEPLOYMENT AND VELOCITY CONFIGURATION FOR TDOA/FDOA LOCALIZATION OF A STATIC SOURCE

A. CENTRALIZED LOCALIZATION

Centralized localization is commonly used in the existing localization system with a common reference sensor to obtain

the TDOA measurements. For the centralized sensor pairing, let the i-th receiver be the reference receiver and the others as auxiliary receivers, then the TDOA and FDOA measurements are $\mathbf{r} = [r_{21}, r_{31}, \cdots r_{M1}]$, $\mathbf{f} = [f_{21}, f_{31}, \cdots f_{M1}]$, the variance matrix of measurement matrix $\widehat{\mathbf{z}}$ consisting of $M-1$ measurements can be represented as [26]:

$$\mathbf{\Sigma}_r = 0.5\sigma_r^2\left[\mathbf{I} + \mathbf{1}\mathbf{1}^T\right], \tag{9}$$

$$\mathbf{\Sigma}_f = 0.5\sigma_f^2\left[\mathbf{I} + \mathbf{1}\mathbf{1}^T\right], \tag{10}$$

where $\mathbf{1} \in \mathbb{R}^{M-1}$ is the vector with all entries equal to 1.

As pointed out in [27], arbitrarily selecting a reference sensor does not change the FIM for TDOA-based source localization. Here, we extend it to the FDOA model. Let

Corollary 1: Given the positions of the receivers and source, i.e. given distance r_i and bearing angle $\phi_i \in [0,\ 2\pi)$, the selection of reference receiver have no impact on the FIM of the FDOA.

Proof: Without loss of generality, assume that receiver 1 and 2 are taken as the reference receivers, respectively. Then the FDOA measurements with different reference receivers can be represented as

$$\begin{aligned}\widehat{\mathbf{z}}_{f1} &= \begin{bmatrix}\widehat{z}_{f21} & \widehat{z}_{f31} & \cdots & \widehat{z}_{fM1}\end{bmatrix}^T \\ &= \mathbf{T}_1\begin{bmatrix}\widehat{z}_{f1} & \widehat{z}_{f2} & \cdots & \widehat{z}_{fM}\end{bmatrix}^T, \end{aligned} \tag{11}$$

$$\begin{aligned}\widehat{\mathbf{z}}_{f2} &= \begin{bmatrix}\widehat{z}_{f12} & \widehat{z}_{f32} & \cdots & \widehat{z}_{fM2}\end{bmatrix}^T \\ &= \mathbf{T}_2\begin{bmatrix}\widehat{z}_{f1} & \widehat{z}_{f2} & \cdots & \widehat{z}_{fM}\end{bmatrix}^T, \end{aligned} \tag{12}$$

where $\mathbf{T}_1$ and $\mathbf{T}_2$ are transformation matrices and are all of dimension $(M-1)\times M$. And $\mathbf{T}_1$ and $\mathbf{T}_2$ can be represented as

$$\mathbf{T}_1 = \begin{bmatrix} -1 & 1 & 0 & \cdots & 0 \\ -1 & 0 & \ddots & \ddots & \vdots \\ \vdots & \vdots & \ddots & \ddots & 0 \\ -1 & 0 & \cdots & 0 & 1 \end{bmatrix},$$

$$\mathbf{T}_2 = \begin{bmatrix} 1 & -1 & 0 & \cdots & 0 \\ 0 & -1 & 1 & 0 & \vdots \\ \vdots & \vdots & 0 & \ddots & 0 \\ 0 & -1 & 0 & 0 & 1 \end{bmatrix}.$$

We can see that through an element transformation matrix, $\mathbf{T}_2$ can be transformed into $\mathbf{T}_1$, i.e.,

$$\mathbf{T}_2 = \mathbf{U}_{21}\mathbf{T}_1, \tag{13}$$

where, $\mathbf{U}_{21}$ is an $(M-1)\times(M-1)$ elementary transformation matrix.

Let $\mathbf{\Sigma}_{f1}, \mathbf{\Sigma}_{f2}$ denote the covariance with different reference receivers. It is easy to obtain that

$$\frac{\partial \mathbf{z}_{f2}}{\partial \mathbf{x}_p} = \frac{\partial \mathbf{z}_{f1}}{\partial \mathbf{x}_p}\mathbf{U}_{21}^T, \tag{14}$$

$$\mathbf{\Sigma}_{f2} = \mathbf{U}_{21}\mathbf{\Sigma}_{f1}\mathbf{U}_{21}^T. \tag{15}$$

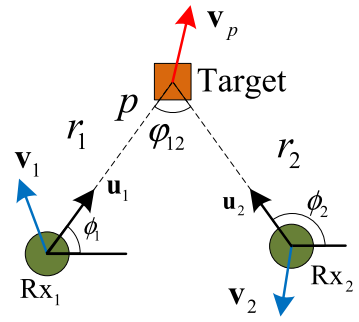

FIGURE 1. Geometry and vector notations for moving source location.

Then $\mathbf{J}^{f2}$ can be written as

$$\begin{aligned}\mathbf{J}^{f2} &= \frac{\partial \mathbf{z}_{f2}}{\partial \mathbf{x}_p}\mathbf{\Sigma}_{f2}^{-1}\left(\frac{\partial \mathbf{z}_{f2}}{\partial \mathbf{x}_p}\right)^T \\ &= \frac{\partial \mathbf{z}_{f1}}{\partial \mathbf{x}_p}\mathbf{U}_{21}^T\left(\mathbf{U}_{21}\mathbf{\Sigma}_{f1}\mathbf{U}_{21}^T\right)^{-1}\left(\frac{\partial \mathbf{z}_{f1}}{\partial \mathbf{x}_p}\mathbf{U}_{21}^T\right)^T \\ &= \frac{\partial \mathbf{z}_{f1}}{\partial \mathbf{x}_p}\left(\mathbf{U}_{21}^T\left(\mathbf{U}_{21}^T\right)^{-1}\right)\mathbf{\Sigma}_{f1}^{-1}\left(\left(\mathbf{U}_{21}^T\right)^{-1}\mathbf{U}_{21}^T\right)\left(\frac{\partial \mathbf{z}_{f1}}{\partial \mathbf{x}_p}\right)^T \\ &= \frac{\partial \mathbf{z}_{f1}}{\partial \mathbf{x}_p}\mathbf{\Sigma}_{f1}^{-1}\left(\frac{\partial \mathbf{z}_{f1}}{\partial \mathbf{x}_p}\right)^T \\ &= \mathbf{J}^{f1}. \end{aligned} \tag{16}$$

Therefore, the selection of reference receiver has no impact on the FIM of the FDOA. For convenience, in this paper, the 1-st receiver is the reference receiver. In static source scenario, i.e. $\mathbf{v}_p = [0, 0]^T$, then the FDOA measurement is given by

$$\begin{aligned} f_{i1} &= \frac{f_0}{c}\left(\mathbf{v}_i^T\mathbf{u}_i - \mathbf{v}_1^T\mathbf{u}_1\right) \\ &= \frac{f_0}{c}\left(v_i\cos\phi_i - v_1\cos\phi_1\right), \quad i = 2, \cdots M. \end{aligned} \tag{17}$$

The partial derivative $\partial f_{i1}/\partial x_p$ can be written as

$$\begin{aligned}\frac{\partial f_{i1}}{\partial x_p} &= \frac{f_0}{c}\left(\frac{\left(y_p - y_i\right)\left(\left(y_i - y_p\right)v_{ix} + \left(x_p - x_i\right)v_{iy}\right)}{\left\|\mathbf{x}_p - \mathbf{x}_i\right\|^3}\right. \\ &\quad \left. - \frac{\left(y_p - y_1\right)\left(\left(y_1 - y_p\right)v_{1x} + \left(p_x - p_{1x}\right)v_{1y}\right)}{\left\|\mathbf{x}_p - \mathbf{x}_1\right\|^3}\right) \\ &= \frac{f_0}{c}\left(\frac{v_{1x}\sin^2\phi_1 - v_{1y}\sin\phi_1\cos\phi_1}{r_1}\right. \\ &\quad \left. - \frac{v_{ix}\sin^2\phi_i - v_{iy}\sin\phi_i\cos\phi_i}{r_i}\right) \\ &= \frac{f_0}{c}\left(\frac{v_{1x}\sin\phi_1 - v_{1y}\cos\phi_1}{r_1}\sin\phi_1\right. \\ &\quad \left. - \frac{v_{ix}\sin\phi_i - v_{iy}\cos\phi_i}{r_i}\sin\phi_i\right) \\ &= \frac{f_0}{c}\left(\omega_i\sin\phi_i - \omega_1\sin\phi_1\right), \end{aligned} \tag{18}$$

where $\omega_i = \frac{v_{ix}\sin\phi_i - v_{iy}\cos\phi_i}{r_i}$ is the angular velocity of the i-th sensor with respect to the source. From Fig. 1, it is obvious

that when $\omega_i > 0$, the sensor is in anti-clockwise rotation. When $\omega_i < 0$, the sensor is in clockwise rotation. Similarly, we have

$$\frac{\partial f_{i1}}{\partial p_y} = \frac{f_0}{c}(\omega_1 \cos\phi_1 - \omega_i \cos\phi_i). \tag{19}$$

Then the FIM of FDOA is given by

$$\mathbf{J}_{F\_\text{static}} = \mathbf{G}\boldsymbol{\Sigma}_f^{-1}\mathbf{G}^T, \tag{20}$$

with

$$\mathbf{G} = \left[g_{ij}, \ldots\right]_{\{i,j\}\in\mathcal{I}_c}, \tag{21}$$

$$g_{ij} = g_i - g_j, \tag{22}$$

$$g_i = \begin{bmatrix} \omega_i \sin\phi_i \\ -\omega_i \cos\phi_i \end{bmatrix}, \tag{23}$$

where $\mathcal{I}_c = [\{2,1\},\{3,1\},\ldots,\{M,1\}]$. Thus the explicit expression of FIM of FDOA can be written as

$$\mathbf{J}_{TF\_\text{static}} = \frac{2}{\sigma_f^2}\begin{bmatrix} \sum_{i=1}^{M}\omega_i^2\sin^2(\phi_i) - \frac{1}{M}\left(\sum_{i=1}^{M}\omega_i\sin\phi_i\right)^2 & \frac{1}{M}\sum_{i=1}^{M}\omega_i\cos\phi_i\sum_{i=1}^{M}\omega_i\sin\phi_i - \sum_{i=1}^{M}\omega_i^2\cos(\phi_i)\sin(\phi_i) \\ \frac{1}{M}\sum_{i=1}^{M}\omega_i\cos\phi_i\sum_{i=1}^{M}\omega_i\sin\phi_i - \sum_{i=1}^{M}\omega_i^2\cos(\phi_i)\sin(\phi_i) & \sum_{i=1}^{M}\omega_i^2\cos^2(\phi_i) - \frac{1}{M}\left(\sum_{i=1}^{M}\omega_i\cos\phi_i\right)^2 \end{bmatrix}. \tag{24}$$

Given the TDOA/FDOA measurement vector $\widehat{\mathbf{z}}$, the FIM, i.e., $\mathbf{J}_{TF\_\text{static}}$, for hybrid TDOA/FDOA-based localization of a static source is given by (25), as shown at the top of the next page, where $\nabla_{\mathbf{x}_p}\mathbf{r}(\mathbf{x}_p)^T\boldsymbol{\Sigma}_r^{-1}\nabla_{\mathbf{x}_p}\mathbf{r}(\mathbf{x}_p)$ is the FIM of TDOA measurement which appears in [28] by Lui et.al.

When $M = 2$, the FIM can be simplified into (26), as shown at the top of the next page.

Corollary 2: Consider the centralized source localization with hybrid TDOA and FDOA measurements with two sensor platforms. ω_1, ω_2 denote the angular velocities, whose magnitude is $\omega_{\max}$. ϕ_1, ϕ_2 denote the bearing angles. Then the optimal deployment and the velocity configuration is

$$\phi_1 - \phi_2 = \pm\pi, \quad \omega_1\omega_2 > 0. \tag{27}$$

Proof: According to (26), the determinant of FIM can be written as

$$\det(\mathbf{J}_{TF\_\text{static}}) = (\omega_1+\omega_2)^2(\cos(\phi_1-\phi_2)-1)^2/\sigma_r^2\sigma_f^2. \tag{28}$$

Then using the D-optimality criterion, we obtain the following optimization problem

$$\arg\max_{\omega_1,\omega_2,\phi_1,\phi_2} (\omega_1+\omega_2)^2(\cos(\phi_1-\phi_2)-1)^2, \tag{29}$$

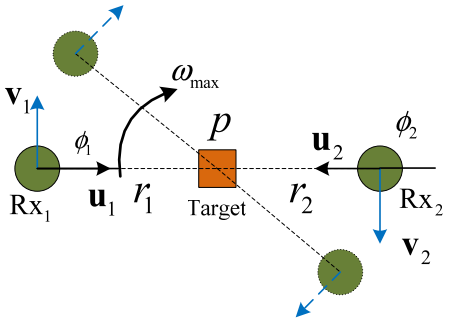

FIGURE 2. Optimal deployment and velocity configuration for centralized localization with two sensors.

which implies $\phi_1 - \phi_2 = \pi, \omega_1\omega_2 > 0$. Therefore, the optimal deployment is a 180° bearing angle separation between the two platforms. And the angular velocities ω_1, ω_2 should be in the same direction of rotation. It is clear that as the angular velocity increases, the localization accuracy improves.

Example 1: Combining the optimal deployment and the angular velocity, a stable deployment is obtained when $\omega_1 = \omega_2 = \omega_{\max}$. Fig. 2 provides an illustration of the optimal sensor deployment, it is important to note that the optimal deployment of two platforms do not depend on the angular velocities, i.e., ω_1, ω_2. However, when $M > 2$, the problem becomes more complicated and we will show that the optimal sensor angular separations are related to the angular velocities.

Corollary 3: Consider the centralized source localization with hybrid TDOA and FDOA measurements with M sensor platforms. Given the angular velocities, i.e., $\omega_1, \omega_2, \cdots, \omega_M$, the determinant is upper bounded by $\left(M^2\Big/\sigma_r^2 + \sum_{i=1}^{M}\omega_i^2\Big/\sigma_f^2\right)^2$, which is achieved if and only if

$$\begin{aligned} \sum_{i=1}^{M}\cos\phi_i = \sum_{i=1}^{M}\sin\phi_i = \sum_{i=1}^{M}\sin(2\phi_i) \\ = \sum_{i=1}^{M}\cos(2\phi_i) = 0, \\ \sum_{i=1}^{M}\omega_i\cos\phi_i = \sum_{i=1}^{M}\omega_i\sin\phi_i = \sum_{i=1}^{M}\omega_i^2\cos 2\phi_i \\ = \sum_{i=1}^{M}\omega_i^2\sin 2\phi_i = 0. \end{aligned} \tag{30}$$

From the upper bound and the optimal conditions, the optimal deployment and velocity of sensors are related to the angular separations and the angular velocities. For the sensors with fixed velocity, the angular velocities vary with the velocity direction and the range between the sensor and the source. For given velocities of UAVs, $\omega_1 = \omega_2 = \ldots, = \omega_{\max}$ can be acquired with minimum distance between sensors and the source.

$$
\begin{aligned}
&\mathbf{J}_{TF\_\text{static}} \\
&= \nabla_{\mathbf{x}_p}\mathbf{r}(\mathbf{x}_p)^T\boldsymbol{\Sigma}_r^{-1}\nabla_{\mathbf{x}_p}\mathbf{r}(\mathbf{x}_p) + \nabla_{\mathbf{x}_p}\mathbf{f}(\mathbf{x}_p)^T\boldsymbol{\Sigma}_f^{-1}\nabla_{\mathbf{x}_p}\mathbf{f}(\mathbf{x}_p) \\
&= 2\begin{bmatrix}
\frac{1}{\sigma_r^2}\sum_{i=1}^{M}\cos^2(\phi_i) - \frac{1}{M\sigma_r^2}\left(\sum_{i=1}^{M}\cos\phi_i\right)^2 + \frac{1}{\sigma_f^2}\sum_{i=1}^{M}\omega_i^2\sin^2(\phi_i) - \frac{1}{M\sigma_f^2}\left(\sum_{i=1}^{M}\omega_i\sin\phi_i\right)^2 \\
\frac{1}{\sigma_r^2}\sum_{i=1}^{M}\cos(\phi_i)\sin(\phi_i) - \frac{1}{M\sigma_r^2}\sum_{i=1}^{M}\cos\phi_i\sum_{i=1}^{M}\sin\phi_i + \frac{1}{M\sigma_f^2}\sum_{i=1}^{M}\omega_i\cos\phi_i\sum_{i=1}^{M}\omega_i\sin\phi_i - \frac{1}{\sigma_f^2}\sum_{i=1}^{M}\omega_i^2\cos(\phi_i)\sin(\phi_i) \\
\frac{1}{\sigma_r^2}\sum_{i=1}^{M}\cos(\phi_i)\sin(\phi_i) - \frac{1}{M\sigma_r^2}\sum_{i=1}^{M}\cos\phi_i\sum_{i=1}^{M}\sin\phi_i + \frac{1}{M\sigma_f^2}\sum_{i=1}^{M}\omega_i\cos\phi_i\sum_{i=1}^{M}\omega_i\sin\phi_i - \frac{1}{\sigma_f^2}\sum_{i=1}^{M}\omega_i^2\cos(\phi_i)\sin(\phi_i) \\
\frac{1}{\sigma_r^2}\sum_{i=1}^{M}\sin^2(\phi_i) - \frac{1}{M\sigma_r^2}\left(\sum_{i=1}^{M}\sin\phi_i\right)^2 + \frac{1}{\sigma_f^2}\sum_{i=1}^{M}\omega_i^2\cos^2(\phi_i) - \frac{1}{M\sigma_f^2}\left(\sum_{i=1}^{M}\omega_i\cos\phi_i\right)^2
\end{bmatrix},
\end{aligned}
\tag{25}
$$

$$
\mathbf{J}_{TF\_\text{static}} = \begin{bmatrix}
\frac{1}{\sigma_r^2}(\cos\phi_1-\cos\phi_2)^2 + \frac{1}{\sigma_f^2}(\omega_1\sin\phi_1-\omega_2\sin\phi_2)^2 \\
\frac{1}{\sigma_r^2}(\cos\phi_1-\cos\phi_2)(\sin\phi_1-\sin\phi_2) - \frac{1}{\sigma_f^2}(\omega_1\cos\phi_1-\omega_2\cos\phi_2)(\omega_1\sin\phi_1-\omega_2\sin\phi_2) \\
\frac{1}{\sigma_r^2}(\cos\phi_1-\cos\phi_2)(\sin\phi_1-\sin\phi_2) - \frac{1}{\sigma_f^2}(\omega_1\cos\phi_1-\omega_2\cos\phi_2)(\omega_1\sin\phi_1-\omega_2\sin\phi_2) \\
\frac{1}{\sigma_r^2}(\sin\phi_1-\sin\phi_2)^2 + \frac{1}{\sigma_f^2}(\omega_1\cos\phi_1-\omega_2\cos\phi_2)^2
\end{bmatrix}.
\tag{26}
$$

$$
\mathbf{J}_{TF\_\text{static}} = \begin{bmatrix}
\sum_{i=1}^{M}\left(\frac{1}{\sigma_r^2}\cos^2(\phi_i) + \frac{1}{\sigma_f^2}\omega^2\sin^2(\phi_i)\right) - \frac{1}{\sigma_r^2 M}\left(\sum_{i=1}^{M}\cos\phi_i\right)^2 - \frac{\omega^2}{\sigma_f^2 M}\left(\sum_{i=1}^{M}\sin\phi_i\right)^2 \\
\left(\frac{1}{\sigma_r^2}-\frac{\omega^2}{\sigma_f^2}\right)\sum_{i=1}^{M}\cos(\phi_i)\sin(\phi_i) - \left(\frac{1}{\sigma_r^2 M}-\frac{\omega^2}{\sigma_f^2 M}\right)\left(\sum_{i=1}^{M}\cos\phi_i\sum_{i=1}^{M}\sin\phi_i\right) \\
\left(\frac{1}{\sigma_r^2}-\frac{\omega^2}{\sigma_f^2}\right)\sum_{i=1}^{M}\cos(\phi_i)\sin(\phi_i) - \left(\frac{1}{\sigma_r^2 M}-\frac{\omega^2}{\sigma_f^2 M}\right)\left(\sum_{i=1}^{M}\cos\phi_i\sum_{i=1}^{M}\sin\phi_i\right) \\
\sum_{i=1}^{M}\left(\frac{1}{\sigma_r^2}\sin^2(\phi_i) + \frac{1}{\sigma_f^2}\omega^2\cos^2(\phi_i)\right) - \frac{1}{\sigma_r^2 M}\left(\sum_{i=1}^{M}\sin\phi_i\right)^2 - \frac{\omega^2}{\sigma_f^2 M}\left(\sum_{i=1}^{M}\cos\phi_i\right)^2
\end{bmatrix}.
\tag{31}
$$

When $\omega_1 = \omega_2 = \ldots, = \omega_{\max}$, $\mathbf{J}_{TF\_\text{static}}$ can be simplified as (31), as shown at the top of this page.

Proposition 1: Consider the centralized source localization with hybrid TDOA and FDOA measurements with M sensor platforms. For equal angular velocities, i.e., $\omega_1 = \omega_i \cdots = \omega_M = \omega_{\max}$, the determinant of FIM is given by $M^2\left(1/\sigma_r^2 + \omega^2/\sigma_f^2\right)^2$.

This upper bound is obtained if and only if

$$
\begin{aligned}
&\sum_{i=1}^{M}\cos\phi_i = 0, \quad \sum_{i=1}^{M}\sin\phi_i = 0, \\
&\sum_{i=1}^{M}\sin(2\phi_i) = 0, \quad \sum_{i=1}^{M}\cos(2\phi_i) = 0.
\end{aligned}
\tag{32}
$$

In this scenario, when $M \geq 3$, it is proved that the receiver distribution with uniform angular arrays (UAAs) can meet the above conditions [28]:

$$
\phi_i = \phi_0 + 2\pi\,(i-1)/M, \quad i = 1, 2, \ldots, M, \tag{33}
$$

where, ϕ_0 is any constant given on $[0, 2\pi/M)$.

Then the minimum value of the determinant is obtained from the uniform angular arrays, which corresponds to an optimal sensor placement strategy in static source scenarios.

Example 2: Combine the optimal deployment and the angular velocity, a stable deployment is obtained with UAAs distribution and $\omega_1 = \omega_i \cdots = \omega_M = \omega_{\max}$. The proposed geometry is stable because the sensors are moving circularly with the same angular velocities, their motion does not

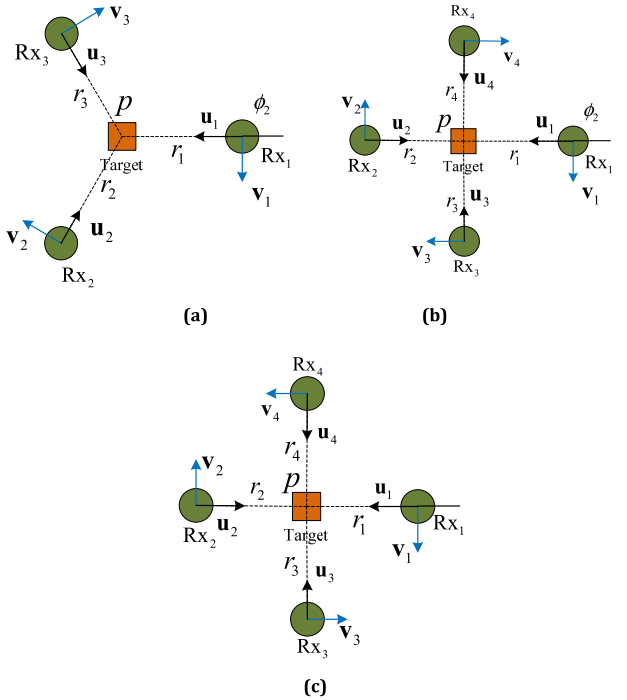

FIGURE 3. Optimal deployment and velocity configuration in centralized localization with $M = 3$, $M = 4$, when $r_i = r_j = r_0$. (a) stable deployment with $M = 3$. (b) stable deployment with $M = 4$. (c) unstable deployment with $M = 4$.

change the relative configuration in all time snapshots. Fig 3. shows the optimal deployment and velocity configuration for $M = 3$, $M = 4$, respectively. When $M \leq 5$, UAAs distribution is the unique solution of formula (32). When $M \geq 6$, even though the optimal deployment is still given by partitions of appropriate angle each with UAAs distribution, the UAAs distribution is one of optimal solutions.

If M is a multiple of 4, i.e., $M = 4k(k = 1, 2, \cdots)$, then another optimal configuration can be acquired with the sensor angular velocities satisfy [29]:

$$\omega_1 = \omega_2 = \cdots = \omega_{M/2} = \omega_{\max}, \tag{34}$$

$$\omega_{M/2+1} = \omega_{M/2+2} = \cdots = \omega_M = -\omega_{\max}. \tag{35}$$

Fig. 3(c) shows the proposed geometry for the optimal sensor deployment that satisfying (30). However, this geometry is unstable when the sensors are moving in the practical application.

B. DECENTRALIZED SENSOR PAIRING

In the centralized localization, communication constraints between the reference sensor and other sensors should be strictly adhered. Therefore, great demands are placed on the communication equipment, especially for large scale sensors. Decentralized sensor pairing localization can be a practical way to settle this problem. No common reference sensor is applied and TDOA/FDOA measurements are collected in pairs after which source location can be calculated between the separated pairs.

Given an even numbers of sensors, which are grouped into $N = M/2$ sensor pairs. Let $\mathcal{I}_1 = [\{i, j\}, \{k, l\}, \cdots]_{\mathcal{I}_1 \in \mathcal{I}, i \neq j \neq k \neq l}$, in decentralized sensor localization, the FIM of TDOA can be given by [30]

$$\mathbf{J}^d_{T\_\text{static}} = \mathbf{G}\boldsymbol{\Sigma}_f^{-1}\mathbf{G}^T, \tag{36}$$

with

$$\mathbf{G} = \left[g_{ij}, g_{kl}, \ldots\right]_{\mathcal{I}_1 \in \mathcal{I}, i \neq j \neq k \neq l}, \tag{37}$$

$$g_{ij} = \begin{bmatrix} \cos\phi_i \\ \sin\phi_i \end{bmatrix}, \tag{38}$$

$$\boldsymbol{\Sigma} = \sigma_r^2 \mathbf{I}. \tag{39}$$

Then the FIM can be written as

$$\mathbf{J}^d_{T\_\text{static}} = \frac{1}{\sigma_r^2}\begin{bmatrix} \sum\limits_{\{i,j\}\in\mathcal{I}_1} \left(\cos\phi_i - \cos\phi_j\right)^2 & \sum\limits_{\{i,j\}\in\mathcal{I}_1} \left(\cos\phi_i - \cos\phi_j\right)\left(\sin\phi_i - \sin\phi_j\right) \\ \sum\limits_{\{i,j\}\in\mathcal{I}_1} \left(\cos\phi_i - \cos\phi_j\right)\left(\sin\phi_i - \sin\phi_j\right) & \sum\limits_{\{i,j\}\in\mathcal{I}_1} \left(\sin\phi_i - \sin\phi_j\right)^2 \end{bmatrix}. \tag{40}$$

Similarly, the FIM of FDOA can be given by

$$\mathbf{J}^d_{F\_\text{static}} = \frac{1}{\sigma_f^2}\begin{bmatrix} \sum\limits_{\{i,j\}\in\mathcal{I}_1} \left(\omega_i\sin\phi_i - \omega_j\sin\phi_j\right)^2 & \sum\limits_{\{i,j\}\in\mathcal{I}_1} \left(\omega_i\sin\phi_i - \omega_j\sin\phi_j\right)\left(\omega_j\cos\phi_j - \omega_i\cos\phi_i\right) \\ \sum\limits_{\{i,j\}\in\mathcal{I}_1} \left(\omega_i\sin\phi_i - \omega_j\sin\phi_j\right)\left(\omega_j\cos\phi_j - \omega_i\cos\phi_i\right) & \sum\limits_{\{i,j\}\in\mathcal{I}_1} \left(\omega_i\cos\phi_i - \omega_j\cos\phi_j\right)^2 \end{bmatrix}. \tag{41}$$

Combine (40) and (41), the hybrid FIM of TDOA and FDOA localization in decentralized sensor pairing can be shown as:

Corollary 4: Consider the decentralized source localization with hybrid TDOA and FDOA measurements with N sensor pairs. For equal angular velocities, i.e., $\omega_1 = \omega_i \cdots = \omega_M = \omega_0$, the determinant of FIM is given by $N^2(1/\sigma_r^2 + \omega_{\max}^2/\sigma_f^2)$, which is attained if and only if

$$\begin{aligned} &\phi_i - \phi_j = \pm\pi, \quad \forall\{i, j\} \in \mathcal{I}_1, \\ &\sum_{\{i,j\}\in\mathcal{I}} \sin 2\phi_i = 0, \quad \sum_{\{i,j\}\in\mathcal{I}} \cos 2\phi_i = 0, \\ &\sum_{\{i,j\}\in\mathcal{I}} \sin^2\phi_i = \sum_{\{i,j\}\in\mathcal{I}} \cos^2\phi_i = N/2. \end{aligned} \tag{43}$$

Proof: The proof is similar to Theorem 2 and is omitted here.

$$\mathbf{J}^{d}_{TF\_static} = \begin{bmatrix} \frac{1}{\sigma_r^2}\sum_{\{i,j\}\in\mathcal{I}_1}\left(\cos\phi_i-\cos\phi_j\right)^2+\frac{1}{\sigma_f^2}\sum_{\{i,j\}\in\mathcal{I}_1}\left(\omega_i\sin\phi_i-\omega_j\sin\phi_j\right)^2 \\ \frac{1}{\sigma_r^2}\sum_{\{i,j\}\in\mathcal{I}_1}\left(\cos\phi_i-\cos\phi_j\right)\left(\sin\phi_i-\sin\phi_j\right)+\frac{1}{\sigma_f^2}\sum_{\{i,j\}\in\mathcal{I}_1}\left(\omega_i\sin\phi_i-\omega_j\sin\phi_j\right)\left(\omega_j\cos\phi_j-\omega_i\cos\phi_i\right) \\ \frac{1}{\sigma_r^2}\sum_{\{i,j\}\in\mathcal{I}_1}\left(\cos\phi_i-\cos\phi_j\right)\left(\sin\phi_i-\sin\phi_j\right)+\frac{1}{\sigma_f^2}\sum_{\{i,j\}\in\mathcal{I}_1}\left(\omega_i\sin\phi_i-\omega_j\sin\phi_j\right)\left(\omega_j\cos\phi_j-\omega_i\cos\phi_i\right) \\ \frac{1}{\sigma_r^2}\sum_{\{i,j\}\in\mathcal{I}_1}\left(\sin\phi_i-\sin\phi_j\right)^2+\frac{1}{\sigma_f^2}\sum_{\{i,j\}\in\mathcal{I}_1}\left(\omega_i\cos\phi_i-\omega_j\cos\phi_j\right)^2 \end{bmatrix}. \quad (42)$$

Example 3: Consider the two sensor pairs in source localization, i.e., $\{1,2\}$ and $\{3,4\}$. For two sensor pairs, it is obvious that the best choice of the intersection angle is $\pi/2$. Combing the optimal deployment and the angular velocity, a stable deployment is also obtained with UAAs distribution, which is shown in Fig 4.

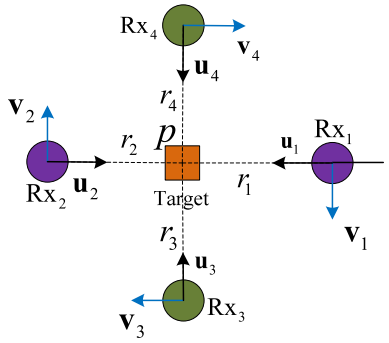

FIGURE 4. Optimal deployment and velocity configuration in decentralized localization with two sensor pairs.

Compared with the centralized localization, the optimal deployment sensor in decentralized localization depends on both the subtended angle by sensor pair $\{i,j\}$ and the angular separation between the sensor pairs based on (42), as shown at the top of this page.

IV. PRELIMINARY ANALYSIS ON OPTIMAL DEPLOYMENT AND VELOCITY CONFIGURATION FOR LOCALIZATION OF A MOVING SOURCE

For moving source localization, the estimated parameters consist of both the source position and velocity. Therefore, the total FIM of both position and velocity in TDOA/FDOA localization is given by

$$\mathbf{J}_{TF\_movable} = \mathbf{H}^T\boldsymbol{\Sigma}\boldsymbol{H} = \begin{bmatrix} \mathbf{H}_{\mathbf{rx}}^T & \mathbf{H}_{\mathbf{fx}}^T \\ \mathbf{H}_{\mathbf{rv}}^T & \mathbf{H}_{\mathbf{fv}}^T \end{bmatrix}\boldsymbol{\Sigma}^{-1}\begin{bmatrix} \mathbf{H}_{\mathbf{rx}} & \mathbf{H}_{\mathbf{rv}} \\ \mathbf{H}_{\mathbf{fx}} & \mathbf{H}_{\mathbf{fv}} \end{bmatrix} = \begin{bmatrix} \mathbf{J}_{\mathbf{rx}}+\mathbf{J}_{\mathbf{fx}} & \mathbf{J}_{\mathbf{fxv}} \\ \mathbf{J}_{\mathbf{fvx}} & \mathbf{J}_{\mathbf{fv}} \end{bmatrix}, \quad (44)$$

where, $\mathbf{H}_{\mathbf{rx}} = \partial\mathbf{r}/\partial\mathbf{p}$, $\mathbf{H}_{\mathbf{rv}} = \partial\mathbf{r}/\partial\dot{\mathbf{p}}$, $\mathbf{H}_{\mathbf{fp}} = \partial\mathbf{f}/\partial\mathbf{p}$, $\mathbf{H}_{\mathbf{fv}} = \partial\mathbf{f}/\partial\dot{\mathbf{p}}$. The FIM of source position is the sum of the matrices $\mathbf{J}_{\mathbf{rx}}$ and $\mathbf{J}_{\mathbf{fx}}$. $\mathbf{J}_{\mathbf{rx}} = \mathbf{H}_{\mathbf{rx}}^T\boldsymbol{\Sigma}_r^{-1}\mathbf{H}_{\mathbf{rx}}$ is an FIM of TDOA measurements for the source position. $\mathbf{J}_{\mathbf{fx}} = \mathbf{H}_{\mathbf{fx}}^T\Sigma_f^{-1}\mathbf{H}_{\mathbf{fx}}$ and $\mathbf{J}_{\mathbf{fv}} = \mathbf{H}_{\mathbf{fv}}^T\boldsymbol{\Sigma}_f^{-1}\mathbf{H}_{\mathbf{fv}}$ are FIMs of FDOA measurements for the source position and velocity, respectively. As shown in (2), TDOAs only depend on the positions of the source and sensors, therefore, TDOAs do not include any information for estimating the source velocity. $\mathbf{J}_{\mathbf{fvx}} = \mathbf{J}_{\mathbf{fxv}}$ are the cross FIMs of FDOA measurements between the source position and velocity.

In movable source scenario, the FDOA between the sensors i and 1 are related as follows:

$$f_{i1} = \frac{f_0}{c}\left(\left(\mathbf{v}_p-\mathbf{v}_i\right)^T\mathbf{u}_i-\left(\mathbf{v}_p-\mathbf{v}_1\right)^T\mathbf{u}_1\right), \quad (45)$$

then the partial derivative $\partial f_{i1}/\partial p_x$ can be written as

$$\begin{aligned}\frac{\partial f_{i1}}{\partial p_x} ==& \frac{f_0}{c}\left(\frac{\left(v_{px}-v_{ix}\right)\sin\phi_i-\left(v_{py}-v_{iy}\right)\cos\phi_i}{r_i}\sin\phi_i\right. \\ &\left.-\frac{\left(v_{px}-v_{1x}\right)v_{1x}\sin\phi_1-\left(v_{py}-v_{1y}\right)\cos\phi_1}{r_1}\sin\phi_1\right) \\ =& \frac{f_0}{c}\left(\tilde{\omega}_1\sin\phi_1-\tilde{\omega}_i\sin\phi_i\right), \end{aligned} \quad (46)$$

with $\tilde{\omega}_1 = \frac{\left(v_{px}-v_{ix}\right)\sin\phi_i-\left(v_{py}-v_{iy}\right)\cos\phi_i}{r_i}$. $\tilde{\omega}_i$ is the relative angular velocity of the i-th sensor with respect to the source

$$\begin{aligned}\tilde{\omega}_i &= \frac{\left(v_{px}-v_{ix}\right)\sin\phi_i-\left(v_{py}-v_{iy}\right)\cos\phi_i}{r_i} \\ &= \frac{v_{px}\sin\phi_i-v_{py}\cos\phi_i}{r_i}-\frac{v_{ix}\sin\phi_i-v_{iy}\cos\phi_i}{r_i} \\ &= v_e\frac{\cos\phi_p\sin\phi_i-\sin\phi_p\cos\phi_i}{r_i}-\omega_i \\ &= \omega_{pi}-\omega_i. \end{aligned} \quad (47)$$

Similarly, we can obtain

$$\frac{\partial f_{i1}}{\partial p_y} = \frac{f_0}{c}\left(\tilde{\omega}_i\cos\phi_i-\tilde{\omega}_1\cos\phi_1\right), \quad (48)$$

$$\tilde{g}_{ij} = \tilde{g}_i-\tilde{g}_j, \quad (49)$$

$$\tilde{g}_i = \begin{bmatrix}\tilde{\omega}_i\sin\phi_i & -\tilde{\omega}_i\cos\phi_i\end{bmatrix}, \quad (50)$$

$$\tilde{\mathbf{G}} = \left[\tilde{g}_{ij},\ldots\right]_{\{i,j\}\in\mathcal{I}}. \quad (51)$$

Then $\mathbf{J}_{TF\_moveable}$ can be rewritten as

$$\mathbf{J}_{TF\_movable} = \begin{bmatrix}\mathbf{G}\boldsymbol{\Sigma}_r^{-1}\mathbf{G}^T+\tilde{\mathbf{G}}\boldsymbol{\Sigma}_f^{-1}\tilde{\mathbf{G}}^T & \mathbf{G}\boldsymbol{\Sigma}_f^{-1}\tilde{\mathbf{G}}^T \\ \mathbf{G}\boldsymbol{\Sigma}_f^{-1}\tilde{\mathbf{G}}^T & \mathbf{G}\boldsymbol{\Sigma}_f^{-1}\mathbf{G}^T\end{bmatrix}. \quad (52)$$

A. OPTIMAL ANGULAR GEOMETRIES AND VELOCITY CONFIGURATION FOR POSITION ESTIMATION

For the centralized sensor pairing, let the 1-st receiver be the reference receiver and others as auxiliary receivers, then the explicit expression of the FIMs for the source position estimation is given by (53), as shown at the top of the next page,

To obtain the optimal deployment and velocity configuration, we aim at obtaining the maximum value of $\det(\mathbf{J_{rx}}+\mathbf{J_{fx}})$, which is corresponding to the position estimate.

1) TWO SENSORS CASE

For two sensors, the determinant is given by

$$\begin{aligned}\det(\mathbf{J_{rx}}+\mathbf{J_{fx}}) &= (\tilde{\omega}_1+\tilde{\omega}_2)^2(\cos(\phi_1-\phi_2)-1)^2/\sigma_r^2\sigma_f^2\\ &= \left(\omega_{p1}+\omega_{p2}-\omega_1-\omega_2\right)^2\\ &\quad\times(\cos(\phi_1-\phi_2)-1)^2/\sigma_r^2\sigma_f^2. \end{aligned}\tag{54}$$

Different from the static scenario, $\tilde{\omega}_i$ is dependent on the relative geometry and source velocity. Without loss of generality, let $\mathbf{v}_p = v_p[0,1]^T$ denote the coordinate reference and the sensor velocities are $\mathbf{v}_1 = v_{\max}[\cos\theta_1, \sin\theta_1]^T$ and $\mathbf{v}_2 = v_{\max}[\cos\theta_2, \sin\theta_2]^T$, respectively. The $\det(\mathbf{J_{rx}}+\mathbf{J_{fx}})$ can be rewritten as

$$\begin{aligned}\det(\mathbf{J_{rx}}+\mathbf{J_{fx}}) &= \left(\left(v_p\cos(\phi_1)+v_{\max}\sin(\phi_1-\theta_1)\right)r_2\right.\\ &\quad\left.+\left(v_p\cos(\phi_2)+v_{\max}\sin(\phi_2-\theta_2)\right)r_1\right)^2\cdot\\ &\quad(\cos(\phi_1-\phi_2)-1)^2/r_1^2r_2^2\sigma_r^2\sigma_f^2. \end{aligned}\tag{55}$$

From above, the maximum value of $\det(\mathbf{J_{rx}}+\mathbf{J_{fx}})$ is determined by the source velocity v_p, sensor velocities $v_{\max}$, bearing angle of the i-th sensor $\phi_i, i\in\{1,2\}$, velocity direction of the i-th sensor $\theta_i, i\in\{1,2\}$ as well as the distance between the i-th sensor and source $r_i, i\in\{1,2\}$. When $r_1=r_2=r$, then $\det(\mathbf{J_{rx}}+\mathbf{J_{fx}})$ can be simplified as

$$\begin{aligned}\det(\mathbf{J_{rx}}+\mathbf{J_{fx}}) &= \left(v_p\cos(\phi_1)+v_{\max}\sin(\phi_1-\theta_1)\right.\\ &\quad\left.+v_p\cos(\phi_2)+v_{\max}\sin(\phi_2-\theta_2)\right)^2\\ &\quad\cdot(\cos(\phi_1-\phi_2)-1)^2/r^2\sigma_r^2\sigma_f^2, \end{aligned}\tag{56}$$

with some trigonometric calculations, the optimization problem to be settled is

$$\begin{aligned}\arg\max f &= 16\sin^4(\phi_1)(v_{te}\cos(\phi_1)\\ &\quad+v_{\max}\sin(\phi_1-\theta_1))^2/r^2\sigma_r^2\sigma_f^2\\ &= 16\sin^4(\phi_1)\left(v_p\cos(\phi_1)+v_{\max}\right)^2/r^2\sigma_r^2\sigma_f^2. \end{aligned}\tag{57}$$

For given v_p and $v_{\max}$, the bearing angle ϕ_1 can be acquired and then the explicit solutions for other parameters are obtained.

Example 4: Consider the two sensors in moving source localization. Let $v_p = 100m/s$,$v_{\max} = 100m/s$ and $r = 1000m$. Fig. 5 shows the optimal deployment of two sensors for position estimation, the optimal angular positions satisfy

$$\begin{aligned}&\phi_1 = \arccos(1/3), \quad \phi_2 = -\arccos(1/3),\\ &\theta_1 = \arccos(1/3)-\pi/2, \quad \theta_2 = -\arccos(1/3)-\pi/2,\\ &\text{or } \phi_1 = \pi-\arccos(1/3), \quad \phi_2 = \arccos(1/3)-\pi,\\ &\theta_1 = \arccos(1/3)-\pi/2, \quad \theta_2 = \arccos(1/3)-\pi/2.\end{aligned}\tag{58}$$

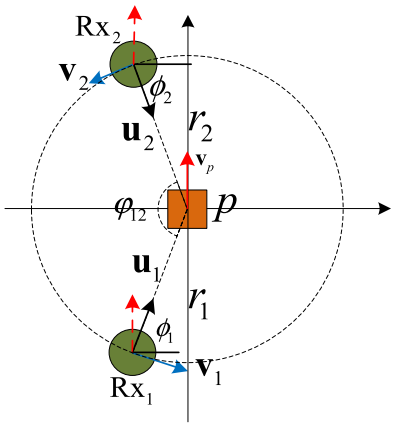

FIGURE 5. Optimal deployment of two sensors for position estimation in movable scenario.

TABLE 1. Optimal angular separation with different source velocities.

Source Velocity v_p (m/s)	Sensor Velocity $v_{\max}$ (m/s)	Optimal angular separation φ_{12} (°)	det(FIM)
1	100	≈180°	0.1599
50	100	156.5547°	0.1784
100	100	140.6850°	0.2246
200	100	128.1377°	0.3676
500	100	117.9075°	1.1035

Different from the static source scenario, the angular position that yields the biggest determinant of the FIM depends on the specific source velocity and sensor velocity. Table 1 lists the optimal angular separation with different source and sensor velocities. For given sensor velocity $v_{\max} = 100m/s$, we can see that when the sensor velocity v_p increases, the angle subtended at the two sensors, i.e., φ_{12} shown in Fig. 5, become smaller, which vary from $2\cos^{-1}(\sqrt{3}/3)\approx 109.47°$ to 180° degrees.

2) ARBITRARY SENSOR CASE

For $M\geq 3$, it is difficult to obtain analytic solutions for the optimal sensor configurations based on A-and D-optimality. Hence, $\mathbf{J_{rx}}+\mathbf{J_{fx}}$ cannot be made diagonal easily and the optimal deployment is related to the relative velocity between the sensor and source. To solve these optimization problems, some traditional optimization algorithms, e.g., gradient search method, sequential quadratic programming (SQP) algorithm and the heuristic algorithms, e.g., differential evolution (DE) algorithm can be applied to obtain a local optima.

B. OPTIMAL DEPLOYMENT FOR VELOCITY ESTIMATION

The explicit expression of FIM of source velocity estimation is given by (59), as shown at the top of the next page.

$$\mathbf{J_{rx}}+\mathbf{J_{fx}} = \begin{bmatrix} \frac{1}{\sigma_r^2}\sum_{i=1}^{M}\cos^2(\phi_i)-\frac{1}{M\sigma_r^2}\left(\sum_{i=1}^{M}\cos\phi_i\right)^2+\frac{1}{\sigma_f^2}\sum_{i=1}^{M}\tilde{\omega}_i^2\sin^2(\phi_i)-\frac{1}{M\sigma_f^2}\left(\sum_{i=1}^{M}\tilde{\omega}_i\sin\phi_i\right)^2 & \\ \frac{1}{\sigma_r^2}\sum_{i=1}^{M}\cos(\phi_i)\sin(\phi_i)-\frac{1}{M\sigma_r^2}\sum_{i=1}^{M}\cos\phi_i\sum_{i=1}^{M}\sin\phi_i+\frac{1}{M\sigma_f^2}\sum_{i=1}^{M}\tilde{\omega}_i\cos\phi_i\sum_{i=1}^{M}\tilde{\omega}_i\sin\phi_i-\frac{1}{\sigma_f^2}\sum_{i=1}^{M}\tilde{\omega}_i^2\cos(\phi_i)\sin(\phi_i) & \\ \frac{1}{\sigma_r^2}\sum_{i=1}^{M}\cos(\phi_i)\sin(\phi_i)-\frac{1}{M\sigma_r^2}\sum_{i=1}^{M}\cos\phi_i\sum_{i=1}^{M}\sin\phi_i+\frac{1}{M\sigma_f^2}\sum_{i=1}^{M}\tilde{\omega}_i\cos\phi_i\sum_{i=1}^{M}\tilde{\omega}_i\sin\phi_i-\frac{1}{\sigma_f^2}\sum_{i=1}^{M}\tilde{\omega}_i^2\cos(\phi_i)\sin(\phi_i) & \\ \frac{1}{\sigma_r^2}\sum_{i=1}^{M}\sin^2(\phi_i)-\frac{1}{M\sigma_r^2}\left(\sum_{i=1}^{M}\sin\phi_i\right)^2+\frac{1}{\sigma_f^2}\sum_{i=1}^{M}\tilde{\omega}_i^2\cos^2(\phi_i)-\frac{1}{M\sigma_f^2}\left(\sum_{i=1}^{M}\tilde{\omega}_i\cos\phi_i\right)^2 & \end{bmatrix}. \tag{53}$$

$$\mathbf{J_{fv}}=\frac{1}{\sigma_f^2}\begin{bmatrix} \sum_{i=1}^{M}\cos^2(\phi_i)-\frac{1}{M}\left(\sum_{i=1}^{M}\cos\phi_i\right)^2 & \sum_{i=1}^{M}\cos(\phi_i)\sin(\phi_i)-\frac{1}{M}\sum_{i=1}^{M}\cos\phi_i\sum_{i=1}^{M}\sin\phi_i \\ \sum_{i=1}^{M}\cos(\phi_i)\sin(\phi_i)-\frac{1}{M}\sum_{i=1}^{M}\cos\phi_i\sum_{i=1}^{M}\sin\phi_i & \sum_{i=1}^{M}\sin^2(\phi_i)-\frac{1}{M}\left(\sum_{i=1}^{M}\sin\phi_i\right)^2 \end{bmatrix} \tag{59}$$

First we notice that the optimal sensor placement for velocity estimation is equivalent to the optimal sensor placement for TDOA localization. Therefore, it is interesting that the optimal sensor placement for the source velocity estimation does not depend on the values of both source and sensor velocities themselves.

C. OPTIMAL ANGULAR GEOMETRIES AND VELOCITY CONFIGURATION FOR POSITION ESTIMATION

From the analysis in section 4.1 and 4.2, the optimal deployment and velocity configuration are different for position estimation and velocity estimation. In real applications, the optimization in source position and velocity are both considered. In 2D scenario, this can be achieved by maximizing the determinant of $\mathbf{J}_{TF}$ in (6) or the trace of $\mathbf{J}_{TF}^{-1}$. However, because of the complexity of $\mathbf{J}_{TF}$, it is difficult to obtain a closed-form expressions. Another way to find the optimal geometries for both position and velocity estimates is cast the contribution of $\det(\mathbf{J_{rx}}+\mathbf{J_{fx}})$ and $\det(\mathbf{J_{fv}})$ using a weighted combination. Hence, such criterion can be used in practice to balance the estimation between the source position and velocity. It is obvious that UAAs distribution is not the optimal deployment in movable source scenario and also the 'optimal deployment' is unstable, which may change rapidly with different source and sensor velocities.

V. PATH PLANNING

Section III and IV give the optimal deployment and velocity configuration in static and movable source scenarios without considering the constraints, respectively. In real applications, if the initial sensor positions present poor geometry, then it takes some time for some mobile sensors to form a better geometry [31].

In this section, we extend our work to the path planning problem [3], [32]–[34]. UAVs are applied in the simulations as moving sensor platforms of hybrid TDOA and FDOA localization to confirm the analytical findings in Section 3 and 4.

Assume the idealized model of a fixed wing UAV dynamic model is [35]:

$$\mathbf{X}_{k+1}=f(\mathbf{X}_k,\mathbf{u}_k),\quad k=1,2,\cdots,M \tag{60}$$

where, $\mathbf{X}_k$ is the system status value $\mathbf{X}_k=[\mathbf{x}_1(k),\cdots,\mathbf{x}_M(k)]^T$ at the time k, and u_k is the control vector $\mathbf{u}_k=[u_1(k),u_2(k),\cdots u_M(k)]$ of UAV at each moment. Without loss of generality, UAV1 is assigned as the reference node, then the proposed waypoint update equation of the UAV is:

$$\mathbf{x}_i(k+1)=\begin{bmatrix}x_i(k)\\ y_i(k)\end{bmatrix}+v_0T\begin{bmatrix}\cos u_i(k)\\ \sin u_i(k)\end{bmatrix} \tag{61}$$

where, v_0 is the UAV flight speed and T is the time interval between waypoint updates. The UAVs path can be optimized by taking the FIM and posterior error covariance as the optimization objective function. Within each time interval, Chan algorithm and EKF are used to update the source position.

$$\begin{cases}\arg\max\ f(\mathbf{u}(k+1))=det(\mathbf{J}_{k+1}(r_i,\theta_i)), & k\le 3\\ \arg\min\ f(\mathbf{u}(k+1))=Tr(\mathbf{P}_{k+1|k+1}(r_i,\theta_i)) & k>3\end{cases} \tag{62}$$

$$s.t.\ \ \|u_i(k+1)-u_i(k)\|\le u_{\max} \tag{63}$$

$$g_{1ij}(\mathbf{u}_k)=R_h-\left\|\mathbf{x}_i(k+1)-\widehat{\mathbf{x}}_t(k)\right\|\ge 0 \tag{64}$$

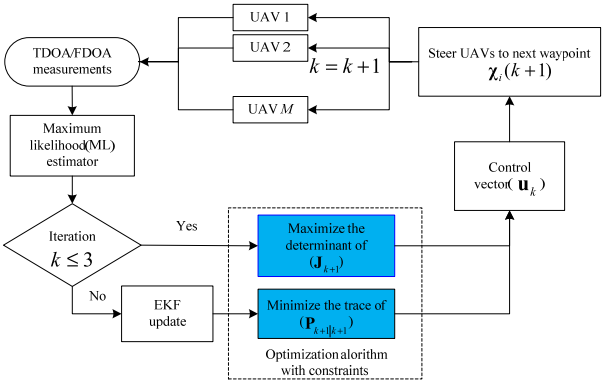

FIGURE 6. Steps of UAV path planning for source localization.

$$g_{2ij}(\mathbf{u}_k) = \left\|\mathbf{x}_i(k+1) - \widehat{\mathbf{x}}_t(k)\right\| - R_l \geq 0 \quad (65)$$

$$g_{3ij}(\mathbf{u}_k) = c_h - \left\|\mathbf{x}_i(k+1) - \mathbf{x}_j(k+1)\right\| \geq 0 \quad (66)$$

$$g_{4ij}(\mathbf{u}_k) = \left\|\mathbf{x}_i(k+1) - \mathbf{x}_j(k+1)\right\| - c_l \geq 0 \quad (67)$$

where, constraint (48) means the turning rate constraint of the platform itself. Conditions (49) and (50) respectively represent the distance constraint from the UAV platform to the source. The upper limit of distance R_h is mainly determined by the receiver signal-to-noise ratio (SNR) and the lower limit R_l is the safe distance between the UAV platform and source. The inequality (51) and (52) are the UAV collision avoidance constraint and communication constraint, respectively.

The optimal sensor placement problems have been formulated as optimal control strategy and parameter optimization problems [36]. Fig. 6 shows the steps of UAV path planning for source localization based on FIM. In this figure, the maximum likelihood (ML) estimator and nonlinear filter are applied to estimation the state of the source based on the hybrid measurements acquired by FDOA and TDOA based sensors. Therefore, the parameters (i.e., ϕ_i, ω_i, r_i, $\mathbf{v}_p$) are acquired, then FIM is also calculated and the control vector U_k is chosen with corresponding to the maximum value of FIM. The path optimization problem is usually under constraints such as turning rate constraint, communication constraint, and minimum distance constraint from the UAVs to the source etc. Then the path planning problem is settled as a nonlinear optimization problem with constraints. Some optimization algorithm, e.g. quadratic programming (SQP) and interior point algorithm, can be utilized. In our work, interior point penalty function method is applied.

VI. SIMULATION RESULTS

The initial source location is $\mathbf{x}_p = [0, 0]^T$, the initial states of UAVs are $\mathbf{x}_1(1) = [-8000, -6000]^T$, $\mathbf{x}_2(1) = [-10000, -6000]^T$, $\mathbf{x}_3(1) = [-10000, -8000]^T$, $\mathbf{x}_4(1) = [-8000, -8000]^T$. The initial heading angles for UAVs are all equal to $\pi/2$ (y axis) with constant velocity $v_{iy} = 100$ km/h ($i = 1, 2, 3, 4$). The sensor noises are $\sigma_r = 1, \sigma_f = 1$, respectively. The time interval between measurements is $T = 1s$. The turning rate constraint is $u_{\max} = 15°$, maximum distance and minimum distance constraint from the UAV platform to the source are $R_h = 20\,km$, $R_l = 0.3\,km$, respectively. UAV communication distance constraint is $c_h = 5\,km$ and collision avoidance constraint is $c_l = 0.2\,km$. The root mean squared error (RMSE) is estimated using 500 Monte Carlo simulations.

A. TDOA/FDOA HYBRID LOCALIZATION IN STATIC SOURCE SCENARIO

In this scenario, the optimized paths of static source localization with different types of localization methods, i.e., centralized localization with and without turning rate constraint, as well as decentralized localization, are investigated. The red triangle denotes the true source location and blue circles are estimations in each time step.

Let UAV1 be the reference station in centralized localization. Fig. 7(a) shows the optimized paths without turning rate constraint, i.e., $-\pi < u_i(K) - U_i(K-1) \leq \pi$ to ascertain effect of UAV velocities. During the first several time steps, UAV2 and UAV4 fly far away from each other to obtain a bigger angular separation, where the initial UAV position present poor configuration. In contrast, UAV1 and UAV3 begin to fly with the zigzag movement patterns. Zigzag movement helps UAVs to acquire good angular velocities of the i-th UAV with respect to the source, which coincides the conclusion in Section 3. After about 200 time steps, the optimal angular separation of 90° is achieved, it is interesting to note that all the UAVs fly toward the source with the zigzag movement patterns.

In Fig. 7(b), the optimized paths are presented with all constraint considered in centralized localization. UAV1 and UAV4 have to keep close to other UAVs within the communication ranges. We also notice that when the UAVs are close to the constraint boundaries or the optimal configurations, they should have changed their flight directions. However, the UAVs are limited to their turning rate constraints. Zigzag movement pattern is unable to be realized and all UAVs tend to fly toward the source until all UAVs fly surround the source.

Fig. 7(c) shows the decentralized sensor pairing localization. UAV1 and UAV2, UAV3 and UAV4 are paired, respectively. The UAVs inside the pairs fly away from each other so that the intersection angles among the sensor pairs are expanded. Compared with the paths in centralized localization shown in Fig. 7(b), there are communication constraints between UAVs, i.e., UAV2 and UAV4, thus in decentralized localization, UAVs can acquire a wider flight region.

Fig. 7(d) shows the localization performance in different types of localization methods, correspondingly. It is clear that the localization performance without constraints has lowest errors at the initial time steps. The localization performance using centralized localization is better than that in the decentralized localization case. Hence, centralized localization can acquire a higher bound of the determinant of the FIM, when compared to decentralized localization. For

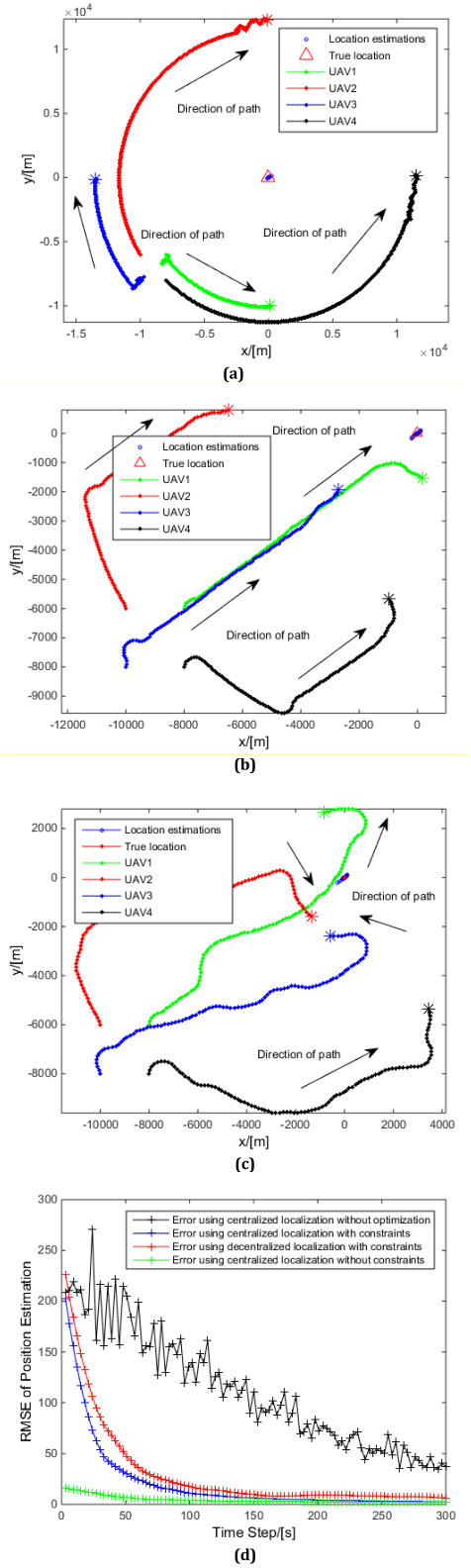

FIGURE 7. Static source scenario. (a) Centralized localization without any constraints. (b) Centralized localization with constraints. (c) Decentralized localization with constraints. (d) RMSE of the source position.

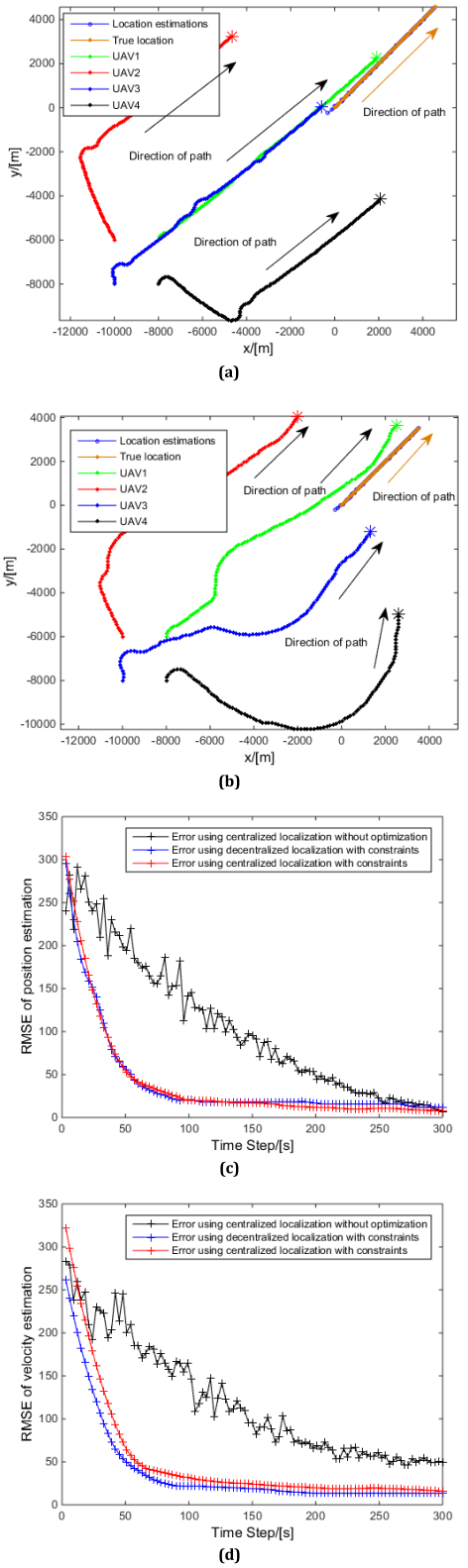

FIGURE 8. Movable source scenario. (a) Centralized localization with constraints. (b) Decentralized localization with constraints. (c) RMSE of the source position. (d) RMSE of the source velocity.

comparison, source localization without the path optimization i.e., straight-line path, is also considered. It is obvious that the localization error without path optimization is large and unstable..

B. TDOA/FDOA HYBRID LOCALIZATION IN MOVABLE SOURCE SCENARIO

In this scenario, the source moves in straight path to the northeast with $V_p = 25m/s$. Figs. 8(a) and (b) show the optimized paths in centralized and decentralized localization, respectively. In the centralized localization, the reference UAV (UAV 1) has to keep communication with the other three UAVs and also they should fly away from each other to obtain a large angular separation. Compared with the static source scenario, UAVs begin to fly toward the direction of the estimated source position after several time steps.

Figs. 8(c) and (d) shows the RMSE of the source position and source velocity respectively. As shown in Figs. 8(c) and (d), the localization performance with path optimization is much better than that in the straight-line path case.

VII. CONCLUSION

In this paper, we have analyzed the sensor deployment and velocity optimization problem in hybrid TDOA and FDOA localization. The FIM was applied to be the optimal criterion of relative sensor-source geometry and velocity. In static source scenario, the centralized and decentralized sensor pairing methods were adopted. It showed that the optimal deployment and velocity configuration were related to both the angular separation and angular velocities. High g-turns of sensor platforms with respect to the source were needed to improve the localization accuracy. In movable source scenario, it was difficult to obtain the optimal deployment and velocity configuration, which varied with different source and source velocities. Some optimization algorithms could be applied to solve the problem when explicit solutions of FIM were not available. Simulations of UAV swarms path planning verified the explicit findings in both static and movable scenarios. Future works will extend the optimal configurations to the 3D scenario and consider the effect of the prior information in a Kalman-type filter.

APPENDIX

Proof of Corollary 3: From the meaning of the FIM, the FIM is always a symmetric positive definite matrix. Let $\lambda_1 > 0$ and $\lambda_2 > 0$ be the two eigenvalues of $\mathbf{J}_{TF\_\text{static}}$, then the eigenvalues of $\mathbf{J}^{-1}_{TF\_\text{static}}$ are $1/\lambda_1$ and $1/\lambda_2$, respectively. According to the Cauchy-Schwarz inequality, we have

$$\begin{aligned}&\left[\sqrt{\lambda_1} \quad \sqrt{\lambda_2}\right]\begin{bmatrix}\sqrt{1/\lambda_1}\\ \sqrt{1/\lambda_2}\end{bmatrix}\\ &\le \sqrt{(\lambda_1+\lambda_2)\,(1/\lambda_1+1/\lambda_2)}\\ &= \sqrt{\left(tr\left(\mathbf{J}_{TF\_\text{static}}\right) tr\left(\mathbf{J}^{-1}_{TF\_\text{static}}\right)\right)} = 2, \end{aligned} \tag{68}$$

Then we have

$$tr\left(\mathbf{J}^{-1}_{TF\_\text{static}}\right) \ge 4/tr\left(\mathbf{J}_{TF\_\text{static}}\right). \tag{69}$$

The inequality holds when $\lambda_1 = \lambda_2 = \lambda$. Since $\mathbf{J}_{TF\_\text{static}}$ is symmetric positive definite, then it implies that $\mathbf{J}_{TF\_\text{static}}$ should be diagonal and

$$\mathbf{J}_{TF\_\text{static}} = \lambda \mathbf{I}. \tag{70}$$

From (25), $tr\left(\mathbf{J}_{TF\_\text{static}}\right)$ is given by

$$\begin{aligned}&Tr\left(\mathbf{J}_{TF\_\text{static}}\right)\\ &= 2\left(\frac{1}{\sigma_t^2}\sum_{i=1}^{M}\cos^2(\phi_i) - \frac{1}{M\sigma_t^2}\left(\sum_{i=1}^{M}\cos\phi_i\right)^2\right.\\ &\quad +\frac{1}{\sigma_f^2}\sum_{i=1}^{M}\omega_i^2\sin^2(\phi_i) - \frac{1}{M\sigma_f^2}\left(\sum_{i=1}^{M}\omega_i\sin\phi_i\right)^2\\ &\quad +\frac{1}{\sigma_t^2}\sum_{i=1}^{M}\sin^2(\phi_i) - \frac{1}{M\sigma_t^2}\left(\sum_{i=1}^{M}\sin\phi_i\right)^2\\ &\quad \left.+\frac{1}{\sigma_f^2}\sum_{i=1}^{M}\omega_i^2\cos^2(\phi_i) - \frac{1}{M\sigma_f^2}\left(\sum_{i=1}^{M}\omega_i\cos\phi_i\right)^2\right)\\ &= 2\left(\frac{M}{\sigma_t^2}+\frac{1}{\sigma_f^2}\sum_{i=1}^{M}\omega_i^2 - \left(\frac{1}{\sigma_t^2 M}\right)\right.\\ &\quad \times\left(\left(\sum_{i=1}^{M}\cos\phi_i\right)^2+\left(\sum_{i=1}^{M}\sin\phi_i\right)^2\right)\\ &\quad \left.-\frac{1}{M\sigma_f^2}\left(\left(\sum_{i=1}^{M}\omega_i\cos\phi_i\right)^2+\left(\sum_{i=1}^{M}\omega_i\sin\phi_i\right)^2\right)\right)\\ &\le 2\left(\frac{M}{\sigma_t^2}+\frac{1}{\sigma_f^2}\sum_{i=1}^{M}\omega_i^2\right) \le 2\left(\frac{1}{\sigma_t^2}+\frac{1}{\sigma_f^2}\sum_{i=1}^{M}\omega_{\max}^2\right). \end{aligned} \tag{71}$$

The inequality holds if and only if

$$\begin{aligned}&\sum_{i=1}^{M}\cos\phi_i = 0, \quad \sum_{i=1}^{M}\sin\phi_i = 0,\\ &\sum_{i=1}^{M}\sin 2\phi_i = 0, \quad \sum_{i=1}^{M}\cos 2\phi_i = 0. \end{aligned} \tag{72}$$

Then combine (70) and (72), we can get

$$\begin{aligned}&\sum_{i=1}^{M}\omega_i\cos\phi_i = 0, \quad \sum_{i=1}^{M}\omega_i\sin\phi_i = 0,\\ &\sum_{i=1}^{M}\omega_i^2\cos 2\phi_i = 0, \quad \sum_{i=1}^{M}\omega_i^2\sin 2\phi_i = 0. \end{aligned} \tag{73}$$

REFERENCES

[1] Y. Zou, H. Liu, W. Xie, and Q. Wan, "Semidefinite programming methods for alleviating sensor position error in TDOA localization," *IEEE Access*, vol. 5, pp. 23111–23120, 2017.
[2] S. Xu and K. Doğançay, "Optimal sensor placement for 3-D angle-of-arrival target localization," *IEEE Trans. Aerosp. Electron. Syst.*, vol. 53, no. 3, pp. 1196–1211, Jun. 2017.
[3] S. A. A. Shahidian and H. Soltanizadeh, "Optimal trajectories for two UAVs in localization of multiple RF sources," *Trans. Inst. Meas. Control*, vol. 38, no. 8, pp. 908–916, 2015.

[4] K. C. Ho and W. Xu, "An accurate algebraic solution for moving source location using TDOA and FDOA measurements," *IEEE Trans. Signal Process.*, vol. 52, no. 9, pp. 2453–2463, Sep. 2004.

[5] N. H. Nguyen and K. Doğançay, "Multistatic pseudolinear target motion analysis using hybrid measurements," *Signal Process.*, vol. 130, pp. 22–36, Jan. 2017.

[6] F. Quo and K. C. Ho, " A quadratic constraint solution method for TDOA and FDOA localization," in *Proc. IEEE Int. Conf. Acoust. Speech Signal Process. (ICASSP)*, May 2011, pp. 2588–2591.

[7] D. Musicki and W. Koch, "Geolocation using TDOA and FDOA measurements," in *Proc. 11th Int. Conf. Inf. Fusion*, Cologne, Germany, Jun./Jul. 2008, pp. 1–8.

[8] D. Musicki, R. Kaune, and W. Koch, "Mobile emitter geolocation and tracking using TDOA and FDOA measurements," *IEEE Trans. Signal Process.*, vol. 58, no. 3, pp. 1863–1874, Mar. 2010.

[9] A. N. Bishop and P. Jensfelt, "An optimality analysis of sensor-target geometries for signal strength based localization," in *Proc. Int. Conf. Intell. Sensors Sensor Netw. Inf. Process. (ISSNIP)*, Melbourne, VIC, Australia, Dec. 2009, pp. 127–132.

[10] A. N. Bishop, B. Fidan, B. D. O. Anderson, K. Doğançay, and P. N. Pathirana, "Optimality analysis of sensor-target localization geometries," *Automatica*, vol. 45, no. 3, pp. 479–492, 2010.

[11] A. N. Bishop, B. Fidan, B. D. O. Anderson, K. Dogancay, and P. N. Pathirana, "Optimality analysis of sensor-target geometries in passive localization: Part 1—Bearing-only localization," in *Proc. 3rd Int. Conf. Intell. Sensors, Sensor Netw. Inf.*, Melbourne, QLD, Australia, Dec. 2007, pp. 7–12.

[12] A. N. Bishop, B. Fidan, B. D. O. Anderson, P. N. Pathirana, and K. Dogancay, "Optimality analysis of sensor-target geometries in passive localization: Part 2—Time-of-arrival based localization," in *Proc. 3rd Int. Conf. Intell. Sensors, Sensor Netw. Inf.*, Melbourne, QLD, Australia, Dec. 2007, pp. 13–18.

[13] B. Yang, "Different sensor placement strategies for TDOA based localization," in *Proc. ICASSP*, Honolulu, HI, USA, Apr. 2007, pp. 1093–1096.

[14] L. Rui and K. C. Ho, "Elliptic localization: Performance study and optimum receiver placement," *IEEE Trans. Signal Process.*, vol. 62, no. 18, pp. 4673–4688, Sep. 2014.

[15] S. Zhao, B. M. Chen, and T. H. Lee, " Optimal sensor placement for target localisation and tracking in 2D and 3D," *Int. J. Control*, vol. 86, no. 10, pp. 1687–1704, 2013.

[16] C. Yang, L. Kaplan, E. Blasch, and M. Bakich, "Optimal placement of heterogeneous sensors for targets with Gaussian priors," *IEEE Trans. Aerosp. Electron. Syst.*, vol. 49, no. 3, pp. 1637–1653, Jul. 2013.

[17] W. Lee, H. Bang, and H. Leeghim, "Cooperative localization between small UAVs using a combination of heterogeneous sensors," *Aerosp. Sci. Technol.*, vol. 27, pp. 105–111, Jun. 2013.

[18] W. Meng, L. Xie, and W. Xiao, "Optimality analysis of sensor-source geometries in heterogeneous sensor networks," *IEEE Trans. Wireless Commun.*, vol. 12, no. 4, pp. 1958–1967, Apr. 2013.

[19] Y. Liang and Y. Jia, "Constrained optimal placements of heterogeneous Range/bearing/RSS sensor networks for source localization with distance-dependent noise," *IEEE Geosci. Remote Sens. Lett.*, vol. 13, no. 11, pp. 1611–1615, Nov. 2016.

[20] M. W. Khan, N. Salman, and A. H. Kemp, "Optimised hybrid localisation with cooperation in wireless sensor networks," *IET Signal Process.*, vol. 11, no. 3, pp. 341–348, 2017.

[21] K. Becker, "Three-dimensional target motion analysis using angle and frequency measurements," *IEEE Trans. Aerosp. Electron. Syst.*, vol. 41, no. 1, pp. 284–301, Jan. 2005.

[22] F. Guo, Y. Fan, C. Xhou, and Q. Li, *Space Electronic Reconnaissance Localization Theories and Methods*. Hoboken, NJ, USA: Wiley, 2014.

[23] D.-G. Kim, Y.-H. Kim, J.-W. Han, and K.-H. Song, "Analysis on the effect of geometric deployment and velocities of sensors based on TDOA/FDOA measurements," in *Proc. Int. Conf. Signal Process. Pattern Recognit.*, 2013, pp. 248–251.

[24] Y.-H. Kim, D.-G. Kim, K.-H. Song, H.-N. Kim, and J. W. Han, "Analysis of sensor-emitter geometry for emitter localisation using TDOA and FDOA measurements," *IET Radar, Sonar Navigat.*, vol. 11, pp. 341–349, Feb. 2017.

[25] H. Hmam, "Optimal sensor velocity configuration for TDOA-FDOA geolocation," *IEEE Trans. Signal Process.*, vol. 65, no. 3, pp. 628–637, Feb. 2017.

[26] B. Yang and J. Scheuing, "Cramer-Rao bound and optimum sensor array for source localization from time differences of arrival," in *Proc. ICASSP*, Philadelphia, PA, USA, Mar. 2005, pp. 961–964.

[27] H. C. So, Y. T. Chan, and F. K. W. Chan, "Closed-form formulae for time-difference-of-arrival estimation," *IEEE Trans. Signal Process.*, vol. 56, no. 6, pp. 2614–2620, Jun. 2008.

[28] K. W. K. Lui and H. C. So, "A study of two-dimensional sensor placement using time-difference-of-arrival measurements," *Digit. Signal Process.*, vol. 19, no. 4, pp. 650–659, Jul. 2009.

[29] M. Hamdollahzadeh, S. Adelipour, and F. Behnia, "Optimal sensor configuration for two dimensional source localization based on TDOA/FDOA measurements," in *Proc. 17th Int. Radar Symp. (IRS)*, May 2016, pp. 1–6.

[30] W. Meng, L. Xie, and W. Xiao, "Optimal TDOA sensor-pair placement with uncertainty in source location," *IEEE Trans. Veh. Technol.*, vol. 65, no. 11, pp. 9260–9271, Nov. 2016.

[31] F. Muñoz, E. S. E. Quesada, H. M. La, S. Salazar, S. Commuri, and L. R. G. Carrillo, "Adaptive consensus algorithms for real-time operation of multi-agent systems affected by switching network events," *Int. J. Robust Nonlinear Control*, vol. 27, no. 9, pp. 1566–1588, 2017.

[32] K. Dogancay, "UAV path planning for passive emitter localization," *IEEE Trans. Aerosp. Electron. Syst.*, vol. 48, no. 2, pp. 1150–1166, Apr. 2012.

[33] K. Dogancay, "Online optimization of receiver trajectories for scan-based emitter localization," *IEEE Trans. Aerosp. Electron. Syst.*, vol. 43, no. 3, pp. 1117–1125, Jul. 2007.

[34] F. Koohifar, A. Kumbhar, and I. Guvenc, "Receding horizon multi-UAV cooperative tracking of moving RF source," *IEEE Commun. Lett.*, vol. 21, no. 6, pp. 1433–1436, Jun. 2017.

[35] P. Sarunic and R. Evans, "Hierarchical model predictive control of UAVs performing multitarget-multisensor tracking," *IEEE Trans. Aerosp. Electron. Syst.*, vol. 50, no. 3, pp. 2253–2268, Jul. 2014.

[36] W. Wang, P. Bai, X. Liang, J. Zhang, and L. He, "Performance analysis for TDOA localization using UAVs with flight disturbances," in *Proc. 20th Int. Conf. Inf. Fusion*, Xi'an, China, Jul. 2017, pp. 1–6.

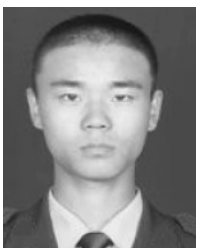

WEIJIA WANG received the B.S. and M.S. degrees from Air Force Engineering University, Xi'an, in 2013 and 2015, respectively, where he is currently pursuing the Ph.D. degree in electronic science and technology with the Air Traffic Control and Navigation College. His research interests include the area of cooperative control of UAV, sensor networks for radar, and electronic warfare applications.

PENG BAI was born in 1961. He received the bachelor's degree in radar engineering from the School of Aeronautics and Astronautics Engineer, Air Force Engineering University, in 1983, and the master's degree in information and communication engineering from the School of Northwestern Polytechnical University, in 1989. He is currently a Professor with the School of Equipment Development and Application Research Center, Air Force Engineering University. He has published more than 120 journal papers as the major author, among them, 30 articles were retrieved by SCI and 37 by EI. His current research interests include advanced electronic science and technology in the future, and science and technology of network information system in the future. He is the Chief Expert and the main person responsible for a number of national key scientific research projects. He received the National Science and Technology Progress award for several times, and he was commended by the President of China.

YUBING WANG was born in 1994. She received the M.S. degree from the Aeronautics and Astronautics Engineering College, Air Force Engineering University, Xi'an, in 2017, where she is currently pursuing the Ph.D. degree with the Air Traffic Control and Navigation College. Her research interests include the area of cooperative control of UAV swarms, wireless sensor networks, and intelligence optimization algorithm.

XIAOLONG LIANG was born in 1981. He received the master's degree in operational research and cybernetics and the Ph.D. degree in armament science and technology from Air Force Engineering University, where he is currently a Professor with the School of Air Traffic Control and Navigation College. He has published more than 50 journal papers and finished more than 20 projects. His research interests include aircraft swarm technology, airspace management intelligence, and intelligent aviation system. He is a major of several national scientific research projects.

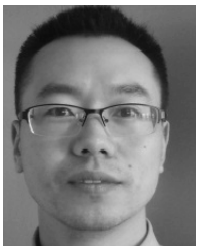

JIAQIANG ZHANG was born in 1984. He received the master's degree in weapon system and application engineering and the Ph.D. degree in armament science and technology from the School of Aeronautics and Astronautics Engineer, Air Force Engineering University, in 2009 and 2012, respectively, where he is currently a Lecturer with the School of Air Traffic Control and Navigation College. He has published more than 20 journal papers and finished more than 10 projects. His research interests include aviation cluster technology and airspace management intelligence.